SPE 92057

Three-Phase Capillary Pressure Correlation for Mixed-Wet Reservoirs

J.O. Helland, SPE, and S.M. Skjæveland, SPE, Stavanger University College

This paper was prepared for presentation at the 2004 SPE International Petroleum Conference in Mexico held in Puebla, Mexico, 8–9 November 2004.

Abstract

We present new three-phase capillary pressure correlations that could be employed to model the dynamics of three-phase transition zones in mixed-wet reservoirs. The capillary pressures are expressed as a sum of two terms. One term is a function of a decreasing saturation and the other term a function of an increasing saturation. Thus the correlations depend on the type of displacement process, i.e., the direction of saturation change. The two-saturation dependency, together with the inclusion of adjustable parameters, ensures that the correlations account for different wettability conditions, saturation histories, and different relationships between the three capillary pressures.

The correlations are compatible with a smooth transition between two- and three-phase flow if one of the phases appears or disappears. In particular, if the gas saturation becomes zero, it is shown that the correlations are reduced to a previously published two-phase correlation validated for oil/water systems in mixed-wet rock.

Capillary pressure curves for various conditions, computed using a previously developed bundle-of-triangular-tubes model, are compared with the correlations, and the match is excellent in all cases. Finally, the correlations are validated experimentally by centrifuge measurements performed on water-wet cores.

Introduction

Three-phase capillary pressure curves are needed to model the dynamics of gas-oil and oil-water transition zone movements in the reservoir. Production from an oil zone causes an upward movement of the oil-water contact and a downward movement of the gas-oil contact. Water may displace oil and gas and gas may displace water and oil. Other scenarios are possible as well. The transition zone dynamics is dominated by capillary-gravity forces and the relationships between the capillary pressures and saturations are required in the entire saturation space.

When solving the equations governing fluid flow in reservoir simulation, the capillary pressure vs. saturation relationship is most conveniently formulated as a simple correlation with adjustable parameters. In the reservoir, situations may occur where one of the phases appears or disappears, e.g., during phase transitions between gas and oil, or when a zero residual oil saturation is approached by drainage through continuous spreading layers in the crevices of the pore space. To implement these scenarios in a numerical reservoir simulator without creating convergence problems, a smooth transition is required between two- and three-phase flow.

In the oil industry three-phase capillary pressure curves have traditionally been predicted from corresponding two-phase measurements. However, experimental work has shown that this practice may not be valid.[1] Moreover, micromodel studies of three-phase flow have revealed that the fluid distribution and the displacement mechanisms at the pore scale may be more complex than for two phases.[2,3] These findings emphasize the need for direct measurements of three-phase capillary pressure curves for various conditions. To our knowledge, measurements with three varying saturations have only been reported by Kalaydjian[4] and, more recently, Virnovsky *et al.*[5] The capillary pressures were measured in water-wet sandstone core samples only. Bradford and Leij[1,6,7] measured three-phase capillary pressures in sandpacks for several wetting conditions achieved by mixing different fractions of water-wet and oil-wet sands. In these experiments, however, one saturation was kept fixed.

In three-phase flow there is an infinite number of possible displacement paths because of two independent saturations. Hence, it is impractical to perform time-consuming measurements of a vast amount of different processes for several rock and fluid properties. This points out the importance of developing physically-based pore-scale network models[8–12] to compute the capillary pressure curves. A pore-scale model, tuned to reproduce the measured data, may be employed to predict capillary pressure curves for other displacement paths not covered by the measurements. A plausible range of values of the parameters to be used in empirical capillary pressure correlations could then be estimated from the computed results for the specific rock and fluid properties under consideration. Such a systematic method based on physical principles to determine

the correlation parameters may improve the reliability of the correlation for use in reservoir simulation.

In this paper we present new three-phase capillary pressure correlations that account for various displacement paths and wettability conditions. It is demonstrated that the correlations are compatible with smooth transitions between two- and three-phase flow. The correlations are compared with the simulation results of a previously developed pore-scale model.[13,14] From these results, we show that the correlation parameters could be correlated to the initial saturations. The correlations are finally validated by recent centrifuge measurements performed on water-wet cores.[5]

Correlations

Among the two-phase capillary pressure correlations reported in the literature, the Brooks-Corey formula is one of the most frequently used because of its simplicity and solid experimental validation.[15] For primary drainage this correlation may be written as

$$P_{cow} = c_w S_w^{-a_w}, \quad . \quad . \quad . \quad . \quad . \quad . \quad . \quad . \quad . \quad . \quad . \quad . \quad . \quad (1)$$

where c_w is the entry pressure, $1/a_w$ the pore-size distribution index, and S_w the normalized water saturation. Skjaeveland *et al.*[16] extended the correlation to account for imbibition, secondary drainage and hysteretic scanning loops for mixed-wet conditions, by using the following reasoning: If Eq. 1 is regarded as valid for a complete water-wet system, then the same functional form should be equally valid for a complete oil-wet system when the subscript w for water is replaced by the subscript o for oil. For intermediate wetting states, both fluids contribute to the overall wettability, and hence the capillary pressure should be modelled as a sum of the water and oil terms, resulting in the correlation

$$P_{cow} = c_w S_w^{-a_w} + c_o S_o^{-a_o}, \quad . \quad . \quad . \quad . \quad . \quad . \quad . \quad . \quad . \quad . \quad . \quad (2)$$

where S_o is the normalized oil saturation. In general, Eq. 2 requires different sets of the parameters a_w, a_o, c_w and c_o for different drainage and imbibition capillary pressure curves. The constants a_w, a_o and c_w are positive, while c_o is negative.

The Brooks-Corey formula is used as a basis for the design of the three-phase capillary pressure correlation because of its extensive validation for two phases.[15,16]

Three-Phase Correlation Design. In three-phase flow there is, for all starting positions in the saturation space, an infinite number of possible ways the three capillary pressures could relate to each other, corresponding to an infinite number of unique saturation trajectories. Thus we assume a process-based approach as a foundation for the correlation development, implying that the processes are known in terms of the saturation trajectories. The processes are sorted into *classes of processes*, defined by how the saturations change. We let the capital letters I, D and C denote increasing, decreasing and constant saturations, respectively. A class of processes is then denoted by a three-letter symbol where the first letter denotes the direction of water saturation change, the second letter denotes the oil saturation change, and the third letter denotes the gas saturation change. This is the same notation as employed by Oak.[17,18]

We propose to formulate three-phase correlations for each process class as a sum of two Brooks-Corey terms, with one term as a function of a decreasing saturation and the other term as a function of an increasing saturation. The two terms should then dominate in different regions of the saturation space. For all the classes of processes the proposed correlations for the three capillary pressures, P_{cij}, $ij = go, ow, gw$, are formulated as follows:

- The process classes XDI and XID where X = I, D or C:

$$P_{cij} = c_g(1 - S_g)^{-a_g} + c_o(1 - S_o)^{-a_o}. \quad . \quad . \quad . \quad (3)$$

- The process classes IXD and DXI where X = I, D or C:

$$P_{cij} = c_g(1 - S_g)^{-a_g} + c_w(1 - S_w)^{-a_w}. \quad . \quad . \quad . \quad (4)$$

- The process classes DIX and IDX where X = I, D or C:

$$P_{cij} = c_o(1 - S_o)^{-a_o} + c_w(1 - S_w)^{-a_w}. \quad . \quad . \quad . \quad (5)$$

The parameters a and c have to be determined. By definition, the three capillary pressures are related by

$$P_{cgw} = P_{cgo} + P_{cow}. \quad . \quad . \quad . \quad . \quad . \quad . \quad . \quad . \quad . \quad . \quad . \quad (6)$$

Hence, correlations are needed only for two of the capillary pressures. This yields a total number of 8 parameters to be determined for each process. In some cases it may be necessary to include residual saturations as correlation parameters as well. The reason for using the functional form $(1 - S_i)$ instead of S_i for phase i in the correlations is that the former allows for positive values of a_i without having capillary pressures starting from plus or minus infinity when $S_i = 0$ initially. Notice also that the functional forms of the correlations are equal for all the three capillary pressures for a given process. The differences in the saturation dependencies and the capillary levels are included by using different values of the a's and the c's.

In the above formulation, Eqs. 3–5, it is stated that two different correlations could be used for processes where all the three saturations are changing. Since the capillary pressures are modelled as functions of two saturations, the actual choice of correlation is indifferent as long as the two saturation terms dominate in different regions of the saturation space. However, if only one of the phases is displaced by the invading phase initially, then the correlation with saturation terms of both the displaced and invading phase should be used.

For implementation in reservoir simulators the capillary pressures are required in the entire saturation space. According to Eqs. 3–5, this could be achieved by specifying the a- and c-parameters as functions of initial saturations for each class of processes. The relationship between initial and residual saturations[19] is well established, and it has been shown theoretically that the parameters in Eq. 1 are related to the irreducible saturation in drainage of a water-wet two-phase system.[20] This implies that a relation between the a- and c-parameters and the initial saturations may exist. Furthermore, the correlation parameters depend in general on the pore network, the saturation

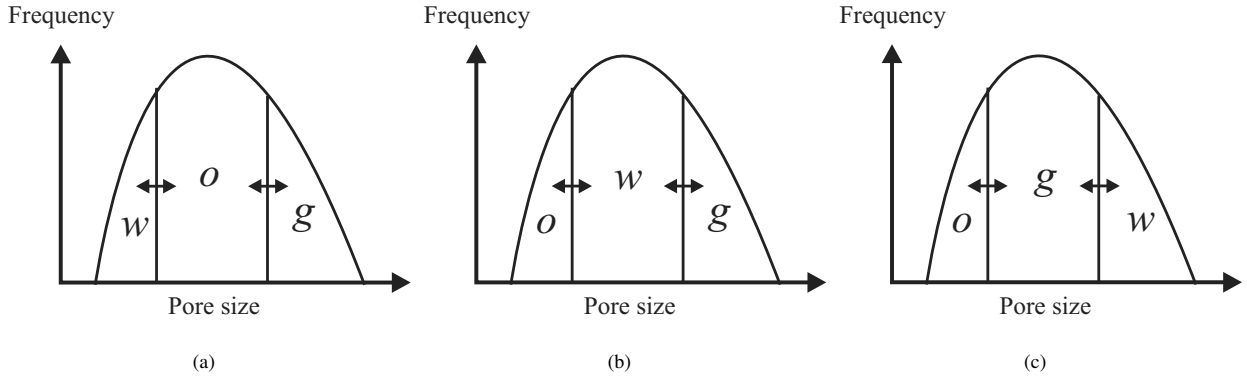

Figure 1: Illustration of pore occupancies for the three generic cases of wetting sequences in three-phase flow. (a) Water-wet case. (b) Weakly oil-wet case. (c) Strongly oil-wet case.

history, the displacement path, the interfacial tensions and the wettability.

The Effects Of Wettability. The wetting order in a three-phase system of water, oil and gas may be divided into three categories:[21,22]

- In *water-wet* media, water is wetting, oil intermediate-wetting, and gas non-wetting. The contact angles satisfy $\theta_{ow} \leq \frac{\pi}{2}$, $\theta_{go} \leq \frac{\pi}{2}$, and $\theta_{gw} \leq \frac{\pi}{2}$.
- In *weakly oil-wet* media, oil is wetting, water intermediate-wetting, and gas non-wetting. The contact angles satisfy $\theta_{ow} > \frac{\pi}{2}$, $\theta_{go} \leq \frac{\pi}{2}$, and $\theta_{gw} \leq \frac{\pi}{2}$.
- In *strongly oil-wet* media oil is wetting, gas intermediate-wetting, and water non-wetting. The contact angles satisfy $\theta_{ow} > \frac{\pi}{2}$, $\theta_{go} \leq \frac{\pi}{2}$, and $\theta_{gw} > \frac{\pi}{2}$.

A rough estimate of the saturation dependencies of the capillary pressures could be performed by studying a simple pore occupancy plot for the three wetting orders, see **Fig. 1**. Residual saturations are not included in the illustrations. We consider displacement paths for invasion of the intermediate-wet phase to clarify how wettability may affect the correlation parameters of Eqs. 3–5.

In water-wet systems, as shown in **Fig. 1 (a)**, oil preferentially invades the intermediate-sized pores, with water and gas present in the smaller and the larger pores, respectively. In this case the gas-oil and oil-water capillary pressures may be estimated as functions of mainly one saturation in the three-phase region of the saturation space:

$$P_{cgo} = P_{cgo}(S_g), \quad P_{cow} = P_{cow}(S_w). \quad . \quad . \quad . \quad . \quad . \quad (7)$$

Oil invasion may be an XID process and hence Eq. 3 is employed to model the capillary pressures. By Eq. 7, the gas-oil capillary pressure could be estimated with $c_o, a_o = 0$, resulting in the expression

$$P_{cij} = c_g(1 - S_g)^{-a_g}, \quad c_g, a_g > 0. \quad . \quad . \quad . \quad . \quad . \quad . \quad (8)$$

The oil-water capillary pressure is given by Eq. 3 with both terms included, and the parameters generally satisfy $c_g, a_g < 0$ and $c_o, a_o > 0$. The gas-water capillary pressure is a function of two saturations and could finally be calculated from Eq. 6.

In weakly oil-wet systems, water preferentially invades the intermediate-sized pores, with oil now present in the smaller pores and gas present in the larger ones, as shown in **Fig. 1 (b)**. In this case the gas-water and oil-water capillary pressures may be approximated as functions of one saturation in the following manner:

$$P_{cow} = P_{cow}(S_o), \quad P_{cgw} = P_{cgw}(S_g). \quad . \quad . \quad . \quad . \quad . \quad (9)$$

Water invasion may be an IXD process, and hence Eq. 4 could be used to model the capillary pressures. To match the saturation dependencies for a weakly oil-wet system, given by Eq. 9, the oil-water capillary pressure is modelled by Eq. 4, with the parameters satisfying $c_g, a_w > 0$ and $c_w < 0$. The sign of the parameter a_g depends on the direction of the first segment of the P_{cow}-curve. The gas-water capillary pressure is approximated by Eq. 8. In this case the gas-oil capillary pressure is a function of two saturations.

In strongly oil-wet systems, gas is wetting relative to water. Hence, gas preferentially invades the intermediate-sized pores, with oil still present in the smaller pores and water now occupied in the larger pores, as shown in **Fig. 1 (c)**. In this case the gas-water and gas-oil capillary pressures may be approximated as functions of mainly one saturation in the three-phase saturation space:

$$P_{cgw} = P_{cgw}(S_w), \quad P_{cgo} = P_{cgo}(S_o). \quad . \quad . \quad . \quad . \quad . \quad (10)$$

The oil-water capillary pressure is then a function of two saturations by Eq. 6. Gas invasion may be an XDI process, and hence Eq. 3 could be used to model the gas-water capillary pressure with the parameters $c_g, a_g, a_o > 0$ and $c_o < 0$. By Eq. 10, the gas-oil capillary pressure could be estimated with $c_g, a_g = 0$,

resulting in the expression

$$P_{cij} = c_o(1 - S_o)^{-a_o}, \quad . \quad . \quad . \quad . \quad . \quad . \quad . \quad . \quad . \quad . \quad . \quad . \quad (11)$$

where $c_o > 0$ and $a_o < 0$.

The wetting order of the three phases depends on the interfacial tensions.[22,23] Hence, in some cases the above approximations may be poor, as the interfacial tensions affect the size of the regions of different saturation dependencies in the saturation space.[24] Moreover, reservoir wettability is never uniform, and hence the extended correlations, Eqs. 3–5, should be used instead of the approximations given by Eqs. 8, 11. This is particularly necessary for reservoirs of mixed or fractional wettability where the capillary pressures in general depend on two saturations.[7,14,24] However, the above analysis contributes to a helpful guidance in choosing reasonable values of the correlation parameters for different wetting states when available information is lacking.

Transitions Between Two- And Three-Phase Flow. A transition from three- to two-phase gas-water flow may occur in condensate reservoirs when the pressure decreases below the dewpoint pressure resulting in evaporation of the oil phase. A possible displacement path for such a scenario is path A in **Fig. 2**. It is split into the two segments A_1 and A_2. Path A_1 is a CDI process, and hence the capillary pressures are modelled by Eq. 3. Path A_2 represents a DDI process, and hence the capillary pressures could be modelled by either Eq. 3 or Eq. 4. The three-phase P_{cgw}-curve must smoothly convert to the two-phase curve when the oil saturation becomes zero. If Eq. 4 is employed for path A_2, it is easily shown that P_{cgw} reduces to the following expression when $S_o = 0$:

$$P_{cgw} = c_g S_w^{-a_g} + c_w S_g^{-a_w}. \quad . \quad . \quad . \quad . \quad . \quad . \quad . \quad . \quad . \quad . \quad . \quad (12)$$

This expression for gas-water systems is analogous to the experimentally validated correlation given by Eq. 2 for two-phase oil-water systems. Eq. 12 should be equally valid since the wetting order of gas and water may change depending on the underlying wettability. The parameters satisfy $c_g, a_g, a_w > 0$ and $c_w < 0$.

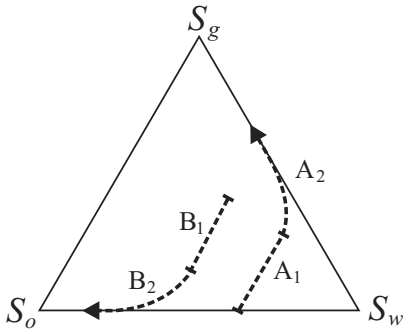

Figure 2: Illustrative examples of displacement paths for transitions from three- to two-phase flow. The oil phase disappears along path A. The gas phase disappears along path B.

Alternatively, the entire path A may be looked upon as a DDI process, and hence Eq. 3 could be used to model the capillary pressures along the trajectory. When $S_o = 0$, the gas-water capillary pressure is reduced to

$$P_{cgw} = c_g S_w^{-a_g} + c_o. \quad . \quad . \quad . \quad . \quad . \quad . \quad . \quad . \quad . \quad . \quad . \quad (13)$$

This expression is consistent with Eq. 12 when the a-parameter of the second term is set to zero. Thus, in many cases Eq. 13 may suffice to describe the two-phase P_{cgw}-curves. The parameters satisfy $c_g, a_g > 0$. The sign of c_o depends on the wetting order of gas and water.

Path B in **Fig. 2** represents a transition process from three- to two-phase oil-water flow. This could occur when the pressure increases above the bubblepoint pressure and gas dissolves in the oil phase. For these processes the three-phase P_{cow}-curve must smoothly change to the two-phase P_{cow}-curve. The segment B_1 represents a CID process, and hence the capillary pressures are modelled by Eq. 3. The segment B_2 represents a DID process, and hence the capillary pressures could be modelled by either Eq. 3 or Eq. 5. Eq. 5 reduces smoothly to the validated two-phase correlation given by Eq. 2 when $S_g = 0$. Alternatively, the entire path B may be considered as a DID process, with the capillary pressures estimated by Eq. 3. In this case the oil-water capillary pressure reduces to

$$P_{cow} = c_g + c_o S_w^{-a_o} \quad . \quad . \quad . \quad . \quad . \quad . \quad . \quad . \quad . \quad . \quad . \quad . \quad (14)$$

when $S_g = 0$. The parameters satisfy $c_o, a_o > 0$. The sign of c_g depends on the wettability. Eq. 14 is consistent with Eq. 2 when the a-parameter of the second term is set to zero. Hence, in many cases Eq. 14 may suffice to describe the two-phase P_{cow}-curve.

Processes tracking the reversed directions of the displacement paths A and B represent examples of transitions from two- to three-phase flow. The reversed direction of path A may represent a process where an increase of pressure results in condensation of the gas phase during water injection. This is an IID process and the capillary pressures are estimated from Eq. 3. The reversed direction of path B may occur when the pressure decreases below the bubblepoint pressure and gas is released. This is an IDI process, and Eq. 3 is used to model the capillary pressures.

Notice that the three-phase correlations, Eqs. 3–5, are employed rather than the two-phase correlations, Eqs. 2, 12, for transition processes where a third phase appears or disappears. This prevents the capillary pressures from approaching infinity when a saturation approaches zero.

Numerical Experiments

A previously developed pore-scale model is employed to compute capillary pressure curves for various processes for different saturation histories and wettability conditions. The correlations are then matched with the simulated results. First we describe the main features of the model. More details can be found elsewhere.[13,14]

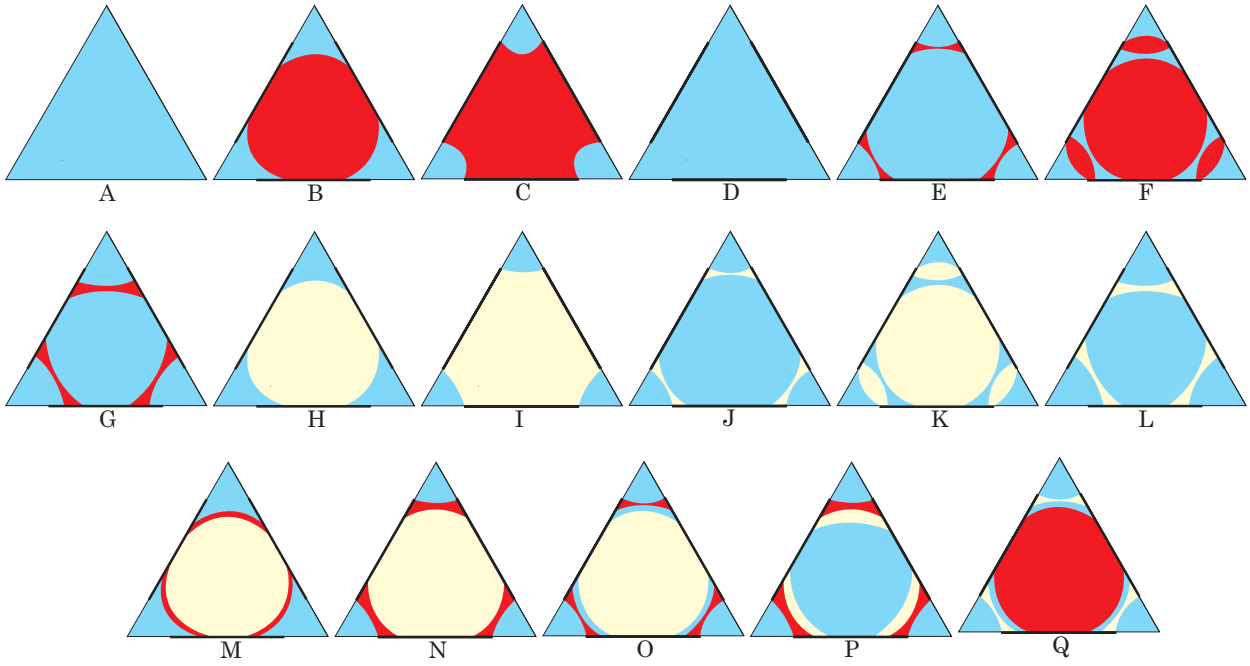

Figure 3: Fluid configurations for any sequences of the invasion processes, with water in blue, oil in red, and gas in yellow. The bold lines along the sides represent the lengths with potentially altered wettability. Oil is always assumed to be wetting relative to gas.

The Pore-Scale Model. The pore network is represented as a bundle of tubes, the tubes having equilateral, triangular, cross-sections. The geometry of the cross-section of a tube is readily described by the half-angle of the corner, $\alpha = 30°$, and the radius of the inscribed circle R. We employ a truncated Weibull distribution to describe the pore-size frequency.[22,25,26] The pore sizes R are selected from the cumulative distribution function in the following manner: Pick random numbers $x \in [0, 1]$ and calculate the inscribed radii from

$$R = R_{\rm ch}\Big(- \ln[(1-x)\exp(-\Big[\frac{R_{\rm max} - R_{\rm min}}{R_{\rm ch}}\Big]^{\eta}) + x]\Big)^{\frac{1}{\eta}} + R_{\rm min}, \quad . \; . \quad (15)$$

where $R_{\rm max}$, $R_{\rm min}$ and $R_{\rm ch}$ are the inscribed radii of the largest, smallest and characteristic pore sizes, respectively, and η is a dimensionless parameter.

The triangular cross-sections allow for the establishment of mixed wettability within a single pore.[22,27] During primary drainage, oil invades the bulk portion of the pores, and hence the sides of the pore walls may be exposed to a change of wettability, while the water-filled corners remain water-wet. To accommodate the contact angle hysteresis between primary drainage, imbibition and secondary drainage,[28,29] we use advancing and receding oil-water contact angles, θ_{owa} and θ_{owr} respectively, that satisfy $\theta_{pd} \le \theta_{owr} \le \theta_{owa}$, where θ_{pd} is the oil-water contact angle during primary drainage.

Van Dijke and Sorbie[23] have proposed the following equations to calculate the gas-oil and gas-water contact angles accounting for the aforementioned wetting orders:

$$\cos\theta_{go} = \frac{1}{2\sigma_{go}}(C_{so}\cos\theta_{ow} + C_{so} + 2\sigma_{go}), \quad . \; . \; . \quad (16a)$$

$$\cos\theta_{gw} = \frac{1}{2\sigma_{gw}}((C_{so} + 2\sigma_{ow})\cos\theta_{ow} + C_{so} + 2\sigma_{go}), \quad (16b)$$

where the equilibrium oil spreading coefficient C_{so} is nonpositive to reflect interfacial tensions measured at thermodynamical equilibrium.[23,30] We calculate the receding gas-oil and gas-water contact angles, θ_{gor} and θ_{gwr} respectively, from Eq. 16 with $\theta_{ow} = \theta_{owr}$, while the advancing contact angles θ_{goa} and θ_{gwa} are calculated from Eq. 16 with $\theta_{ow} = \theta_{owa}$.

The model simulates capillary pressure curves for any sequences of the oil, water and gas invasion processes starting with primary drainage. Different combinations of the contact angles and the capillary pressures then lead to a diversity of possible cross-sectional fluid configurations,[12,14,31] as shown in **Fig. 3**. The bold lines along the sides indicate the lengths with potentially altered wettability. The number of configurations is limited by several assumptions. Oil is always assumed to be wetting relative to gas. We allow at most two interfaces to be present on the surface of altered wettability. A third interface may be present at the position separating water-wet from wettability-altered surface. Because of contact angle hysteresis, all the interfaces are allowed to hinge at fixed positions while the contact angles change with capillary pressure. If the advancing or receding contact angles are reached, the interfaces

	Final configuration		
Initial configuration	Oil invasion	Water invasion	Gas invasion
A	C	–	–
B	C	D or G	H, I or M
C	–	D or E	I or N
D	B or C	–	H or I
E	C or F	D	I, N or O
F	C	E	I, N or O
G	B	D	H, I or M
H	B or C	D or L	I
I	C	D or J	–
J	C or Q	D	I or K
K	C or Q	J	I
L	B or C	D	H
M	B or N	D, G or H	H
N	C	D, E, I, M or P	I
O	C, F or N	E or H	N
P	C or E	E or J	J or N
Q	C	B or J	I or K

Table 1: The programmed direct displacements during the oil, water and gas invasion processes.

begin to move with a constant contact angle during a further change of capillary pressure. We do not study situations where the gas pressure is large enough for gas invasion into tubes, and corners of tubes, where oil has never been. With these assumptions we find that the 17 configurations presented in **Fig. 3** may occur. The curvatures of the gas-oil interfaces depicted in the configurations are always positive, while the gas-water and the oil-water interfaces may have positive or negative curvatures to satisfy Eq. 6.

Van Dijke *et al.*[32,33] have derived general formulas for two- and three-phase capillary entry pressures for piston-like invasion into angular tubes of uniform wettability using an energy balance equation. Recently, this approach has been extended to account for mixed wettability and contact angle hysteresis for triangular tubes.[14,34] Because of the possibility of simultaneous displacements of the fluids occupying the cross-sections and the hinging of the interfaces in the corners during saturation reversals, invasion may not necessarily proceed in the order of monotonic increasing or decreasing pore sizes even for uniform contact angles. We have formulated algorithms to determine the invasion type and the associated capillary pressure for each configuration. All the programmed pore-scale events, i.e., the displacements between the different configurations, are presented in **Table 1**, including both piston-like invasion and the collapse of fluid layers.

Correlations Compared With Simulation Results. We employ the pore-scale model to compute three-phase capillary pressure curves for various conditions. The simulations are performed on a bundle consisting of 2000 tubes. The pore sizes are calculated from Eq. 15 with $R_{\min} = 1\mu$m, $R_{\max} = 100\mu$m, $R_{\rm ch} = 2\mu$m, and $\eta = 1.5$. We consider a fluid system with the interfacial tensions $\sigma_{go} = 0.010$ N/m, $\sigma_{ow} = 0.030$ N/m and $\sigma_{gw} = 0.040$ N/m, representing realistic values for a system of water, crude oil and natural gas.[35] The equilibrium spreading coefficient then satisfies $C_{so} = 0$, which corresponds to a fluid system where the oil has spread between water and gas.[30] The contact angle during primary drainage is set to $\theta_{pd} = 0°$.

We simulate primary drainage followed by waterflooding to establish several initial saturations. Then we simulate gas invasion and subsequent invasion processes. To study classes of processes with two increasing saturations, all the three capillary pressures have to vary. For simplicity we consider processes that obey linear relationships between P_{cow} and P_{cgo}:

$$P_{cgo} = \frac{(P_{cow} - P_{cow}^{\rm init})(P_{cgo}^{\rm end} - P_{cgo}^{\rm init})}{P_{cow}^{\rm end} - P_{cow}^{\rm init}} + P_{cgo}^{\rm init}, \quad . \quad . \quad . \quad (17)$$

where $P_{cij}^{\rm init}$ and $P_{cij}^{\rm end}$, $ij = ow, go$ are the initial and final values of the capillary pressures along the displacement path. The gas-water capillary pressure is calculated from Eq. 6. Processes determined by Eq. 17 are simulated as follows: Specify an array of uniformly decreasing or increasing P_{cow}-values and calculate the corresponding array of P_{cgo}-values from Eq. 17. Then alternate invasion processes of two of the fluids are performed. A specific invasion process is terminated when the next value of the capillary pressure in the array is reached. The saturation and capillary pressure data are recorded at each termination of the invasion processes of one of the fluids.

The three-phase correlations are matched with the computed curves using a standard curvefitting technique to determine the correlation parameters. The main steps in the curvefitting procedure is as follows for a process where phase i displaces phase j: For large saturations S_i the term $c_i(1 - S_i)^{-a_i}$ is fitted to provide estimates of c_i and a_i. Similarly, for large S_j the term $c_j(1-S_j)^{-a_j}$ is fitted to provide estimates of c_j and a_j. Finally, the parameters c_i, a_i, c_j, a_j are optimized simultaneously for the entire displacement path of the specific process. In some cases, however, a better match could be obtained if the initial estimates were determined for the entire displacement path instead.

Gas Invasion And The Effects Of Wettability. We study the P_{cgo}-curves for gas invasion processes at constant P_{cow}-values, i.e., for each process $P_{cow}^{\rm init} = P_{cow}^{\rm end}$ in Eq. 17. Under these circumstances gas invasion may be classified as a DDI or CDI process, and hence Eq. 3 is used to model the capillary pressures. Two generic cases of strongly wetting conditions are studied and contact angle hysteresis is neglected. The contact angles employed for the water-wet case are set to $\theta_{ow} = 30°, \theta_{go} = 0°$ and $\theta_{gw} = 25.9°$. For the strongly oil-wet case the contact angles are set to $\theta_{ow} = 180°, \theta_{go} = 0°$ and $\theta_{gw} = 120°$. The computed saturation trajectories and the gas-oil iso-capillary pressure curves are shown in **Figs. 4**, **5**. Notice that the iso-curves are in agreement with the saturation dependencies of P_{cgo} given by Eqs. 7, 10. The comparisons between the computed P_{cgo}-curves and the correlations are shown in **Fig. 6**.

To analyze how wettability affects the correlation parameters in the *three-phase* saturation space, the curvefitting is ter-

minated at $S_o = 0$ for the water-wet case, and at $S_g = 0.93$ for the oil-wet case. In **Figs. 7**, **8** the correlation parameters are plotted vs. initial water saturation S_{wi} . The parameters c_o, a_o are not shown for the water-wet case, since the estimated values of c_o are in the order of 10^{-4}–10^{-12}, while the values of a_o are in the order of 10^{1}–10^{2}. These results indicate that the oil saturation term is negligible in most of the saturation space, and that the P_{cgo}-curves can be estimated from Eq. 8 as expected. For the oil-wet case both saturation terms of the correlation contribute significantly, even though the gas-oil isocaps indicate that P_{cgo} can be approximated as function of only the oil saturation. The inclusion of both terms seems necessary in this case to model the correct shape of the curves. For both the wetting conditions we have fitted third-order polynomials to the correlation parameters as functions of S_{wi}:

$$p(S_{wi}) = p_3 S_{wi}^3 + p_2 S_{wi}^2 + p_1 S_{wi} + p_0. \quad . \quad . \quad . \quad . \quad (18)$$

Plots of the polynomials are also shown in **Figs. 7**, **8**, and the estimated coefficients are shown in **Table 2**. However, capillary pressure curves for other conditions may exhibit different functional relationships between the correlation parameters and the initial saturations. The main observation in the two examples is that for water-wet conditions the c-parameters decrease with increasing S_{wi}, whereas for oil-wet conditions the c-parameters increase with S_{wi}. The a-parameters exhibit the opposite behavior. This indicates that these relationships may be more complex for nonuniform wettabilities.

		p_0	p_1	p_2	p_3
Water-wet	c_g [Pa]	4173.2	-3943.8	5113.9	-3132.2
	a_g	0.33	2.57	-6.02	6.90
Oil-wet	c_g [Pa]	2721	-847.3	7293	1594
	a_g	3.79	-29.5	74.0	-56.9
	c_o [Pa]	-3612.9	58417	-137549	126839
	a_o	5.44	-57.4	153.8	-137.8

Table 2: The estimated coefficients of the polynomial, Eq. 18.

Results For Mixed-Wet Conditions. To simulate capillary pressure curves for mixed-wet conditions, we assume randomly distributed advancing oil-water contact angles within the range $\theta_{owa} \in [60°, 180°]$. For convenience, the receding contact angles are calculated by $\theta_{owr} = 0.7\theta_{owa}$. The gas-oil and gas-water contact angles are calculated from Eq. 16.

The saturation trajectories and the capillary pressure curves for gas invasion at constant P_{cow} are presented in **Fig. 9**. Eq. 3 is used to model the capillary pressure curves, and the match with the simulations is good for all the displacement paths. The simulations are terminated at $S_g = 0.95$. At this point the oil saturation has become zero for most of the displacement paths. While the curvefitting of P_{cgo} was terminated at $S_o = 0$, the entire trajectories were employed for P_{cgw} to study the transition to two-phase gas-water flow. The good match indicates that the three-phase correlations may be suitable to model processes where one of the phases disappears. After the oil saturation has become zero, the expression for P_{cgw} is reduced to Eq. 13. In this example, the optimized parameters for P_{cgw} satisfy $c_g, a_g, a_o > 0$ and $c_o < 0$, as expected.

We have fitted the capillary pressure curves for different processes initiated from some of the gas invasion trajectories presented in **Fig. 9**. The results for oil invasion at constant P_{cgw} are shown in **Fig. 10**. These displacement paths may be classified as DID processes where the gas saturation becomes zero during the displacement. The capillary pressures are modelled by Eq. 3 which reduces to Eq. 14 when invasion proceeds as a two-phase oil-water displacement.

The results for water invasion initiated from another gas invasion trajectory are presented in **Fig. 11**. During each waterflooding P_{cgo} is constant. Under these circumstances the displacements are classified as IDD processes, and Eq. 4 is employed to model the capillary pressure curves. In this case the gas saturation becomes zero during the processes, and hence the oil-water capillary pressure reduces to

$$P_{cow} = c_g + c_w S_o^{-a_w}, \quad . \quad . \quad . \quad . \quad . \quad . \quad . \quad . \quad . \quad . \quad . \quad . \quad (19)$$

where the optimized parameters satisfy $c_g, a_w > 0$ and $c_w > 0$.

Eq. 17 is employed to study processes with two increasing saturations. For the DII processes we simulate alternate oil and gas invasion processes. In this case the parameters of Eq. 17 satisfy $P_{cow}^{\text{end}} > P_{cow}^{\text{init}}$ and $P_{cgo}^{\text{end}} < P_{cgo}^{\text{init}}$. The saturation and capillary pressure data are recorded after each gas invasion. The simulations are terminated at $S_w = 0.05$. For these processes the capillary pressure curves are modelled by Eq. 5, since the oil saturations increase more than the gas saturations in the last segments of the displacement paths, see **Fig. 12**. Plots of the curvefitting results together with the simulated capillary pressures are also shown in **Fig. 12**.

Continuous WAG-injections may be classified as IDI processes. These processes are simulated with $P_{cow}^{\text{end}} < P_{cow}^{\text{init}}$ and $P_{cgo}^{\text{end}} > P_{cgo}^{\text{init}}$ in Eq. 17. In this case alternate water and gas invasions are simulated, and the saturation and capillary pressure data are recorded after each gas invasion process. The simulations are terminated at $S_o = 0.05$. Eq. 5 is employed to model the capillary pressures, since the water saturations increase more than the gas saturations in the last segments of the displacement paths, see **Fig. 13**. Plots of the curvefitting results together with the simulated capillary pressures are also shown in **Fig. 13**.

Validation By Centrifuge Measurements

The correlations are validated by centrifuge measurements of capillary pressure in water-wet Berea sandstone cores. Gravity drainage by gas is measured in 4 cores at different initial saturations established by primary drainage. For the details concerning the measurements we refer to Virnovsky *et al.*[5] The measured displacement paths represent CDI or DDI processes, and hence Eq. 3 is employed to model the capillary pressures. The displacement paths and the curves fitted to the measured capillary pressure data are shown in **Fig. 14** for all the cores. The match is good in all cases. More measurements for different saturation histories, process types and wetting states are required to provide a more thorough validation of the correlations.

Conclusions

In this paper we have proposed new three-phase capillary pressure correlations for mixed-wet reservoirs. The correlations are composed of two terms, where one term is a function of an increasing saturation and the other term is a function of a decreasing saturation. Hence, the correlations depend on the displacement path, i.e., the direction of saturation change. This two-saturation dependency together with the adjustable parameters ensures that the correlations could be employed to describe capillary pressure curves for various conditions.

The specific conclusions are:

1. It is demonstrated that the correlations are compatible with a smooth transition between two- and three-phase flow.

2. The correlations are compared with the capillary pressure curves for different displacement paths computed from a bundle-of-triangular-tubes model. The match is excellent in all cases. The correlation parameters may be correlated to the initial saturations.

3. The correlations are validated for water-wet conditions by centrifuge measurements of capillary pressure in sandstone cores.

Nomenclature

a = Correlation parameter
c = Correlation parameter
C_s = Equilibrium spreading coefficient
p = Polynomial
p_i = Polynomial coefficients
P = Pressure
R = Radius of the inscribed circle
S = Saturation
x = Random number between 0 and 1
α = Corner half angle
η = Parameter in the Weibull distribution
θ = Contact angle
σ = Interfacial tension

Subscripts

a = Advancing
c = Capillary
ch = Characteristic
g = Gas
i = Initial
max = Maximum
min = Minimum
o = Oil
pd = Primary drainage
r = Receding
w = Water

Superscripts

end = Final
init = Initial

Abbreviations

C = Constant saturation
D = Decreasing saturation
I = Increasing saturation
WAG = Water alternate gas

Acknowledgements

Support for Johan Olav Helland was provided by Statoil through the VISTA program.

References

1. Bradford, S.A. and Leij, F.J.: "Wettability effects on scaling two- and three-fluid capillary pressure-saturation relations," *Env. Sci. Techn.* (1995) **29**, 1446–1455.
2. Øren, P.E. and Pinczewski, W.V.: "Fluid distribution and pore-scale displacement mechanisms in drainage dominated three-phase flow," *Transport in Porous Media* (1995) **20**, 105–133.
3. Keller, A.A., Blunt, M.J., and Roberts, P.V.: "Micromodel observation of the role of oil layers in three-phase flow," *Transport in Porous Media* (1997) **26**, 277–297.
4. Kalaydjian, F.J.-M.: "Performance and analysis of three-phase capillary pressure curves for drainage and imbibition in porous media," paper SPE 24878 presented at the 1992 SPE Annual Technical Conference and Exhibition, Washington, DC, Oct. 4–7.
5. Virnovsky, G.A., Vatne, K.O., Iversen, J.E., and Signy, C.: "Three-phase capillary pressure measurements in centrifuge at reservoir conditions," paper SCA 2004–19 presented at the 2004 International Symposium of the Society of Core Analysts, Abu-Dhabi, U.A.E., Oct. 5–9.
6. Bradford, S.A. and Leij, F.J.: "Fractional wettability effects on two- and three-fluid capillary pressure-saturation relations," *J. Cont. Hydr.* (1995) **20**, 89–109.
7. Bradford, S.A. and Leij, F.J.: "Predicting two-and three-fluid capillary pressure-saturation relationships of porous media with fractional wettability," *Water Resources Research* (1996) **32**, No. 2, 251–259.
8. Mani, V. and Mohanty, K.K.: "Pore-level network modeling of three-phase capillary pressure and relative permeability curves," *SPEJ* (Sept. 1998) 238–248.
9. Øren, P.E., Bakke, S., and Arntzen, O.J.: "Extending predictive capabilities to network models," *SPEJ* (Dec. 1998) 324–336.
10. Lerdahl, T.R., Øren, P.E., and Bakke, S.: "A predictive network model for three-phase flow in porous media," paper SPE 59311 presented at the 2000 SPE/DOE Improved Oil Recovery Symposium, Tulsa, OK, Apr. 3–5.
11. Blunt, M.J., Jackson, M.D., Piri, M., and Valvatne, P.H.: "Detailed physics, predictive capabilities and macroscopic consequences for pore-network models of multiphase flow," *Advances in Water Resources* (2002) **25**, 1069–1089.
12. Piri, M. and Blunt, M.J.: "Pore-scale modeling of three-phase flow in mixed-wet systems," paper SPE 77726 presented at the 2002 SPE Annual Technical Conference and Exhibition, San Antonio, TX, Sept. 29–Oct. 2.
13. Helland, J.O. and Skjæveland, S.M.: "Physically-based capillary pressure correlation for mixed-wet reservoirs from a bundle-of-tubes model," paper SPE 89428 presented at the 2004 SPE/DOE Fourteenth Symposium on Improved Oil Recovery, Tulsa, OK, Apr. 17–21.

14. Helland, J.O. and Skjæveland, S.M.: "Three-phase mixed-wet capillary pressure curves from a bundle-of-triangular-tubes model," paper presented at the 8th International Symposium on Reservoir Wettability, Houston, TX, May 16–18, 2004.
15. Brooks, R.H. and Corey, A.T.: "Hydraulic properties of porous media," Hydraulic paper no. 3, Colorado State University, 1964.
16. Skjaeveland, S.M., Siqveland, L.M., Kjosavik, A., Hammervold Thomas, W.L., and Virnovsky, G.A.: "Capillary pressure correlation for mixed-wet reservoirs," *SPERE* (2000) **3**, No. 1, 60–67.
17. Oak, M.J.: "Three-phase relative permeability of water-wet Berea," paper SPE 20183 presented at the 1990 SPE/DOE Seventh Symposium on Enhanced Oil Recovery, Tulsa, OK, Apr. 22–25.
18. Oak, M.J.: "Three-phase relative permeability of intermediate-wet Berea sandstone," paper SPE 22599 presented at the 1991 SPE Annual Technical Conference and Exhibition, Dallas, TX, Oct. 6–9.
19. Land, C.S.: "Calculation of imbibition relative permeability for two- and three-phase flow from rock properties," *SPEJ* (June 1968) 149–156.
20. Papatzacos, P. and Skjæveland, S.M.: "Relative permeability from thermodynamics," *SPEJ* (March 2004) 47–56.
21. Zhou, D. and Blunt, M.: "Wettability effects in three-phase gravity drainage," *J. Pet. Sci. Eng.* (1998) **20**, 203–211.
22. Hui, M.H. and Blunt, M.J.: "Effects of wettability on three-phase flow in porous media," *J. Phys. Chem. B* (2000) **104**, 3833–3845.
23. van Dijke, M.I.J. and Sorbie, K. S.: "The relation between interfacial tensions and wettability in three-phase systems: Consequences for pore occupancy and relative permeability," *J. Pet. Sci. Eng.* (Apr. 2002) **33**, No. 1–3, 39–48, Special Issue.
24. van Dijke, M.I.J., McDougall, S.R., and Sorbie, K.S.: "Three-phase capillary pressure and relative permeability relationships in mixed-wet systems," *Transport in Porous Media* (2001) **44**, No. 1, 1–32.
25. Diaz, C.E., Chatzis, I., and Dullien, F.A.L.: "Simulation of capillary pressure curves using bond correlated site percolation on a simple cubic network," *Transport in Porous Media* (1987) **2**, 215–240.
26. Fenwick, D.H. and Blunt, M.J.: "Three-dimensional modeling of three phase imbibition and drainage," *Adv. Water Resources* (1998) **25**, No. 2, 121–143.
27. Kovscek, A.R., Wong, H., and Radke, C.J.: "A pore-level scenario for the development of mixed wettability in oil reservoirs," *Am. Inst. Chem. Eng. J.* (1993) **39**, No. 6, 1072–1085.
28. Morrow, N.R.: "The effects of surface roughness on contact angle with special reference to petroleum recovery," *J. Can. Pet. Tech.* (1975) **14**, No. 4, 42–53.
29. Yang, S.-Y., Hirasaki, G.J., Basu, S., and Vaidya, R.: "Mechanisms for contact angle hysteresis and advancing contact angles," *J. Pet. Sci. Eng.* (1999) **24**, 63–73.
30. Blunt, M., Zhou, D., and Fenwick, D.: "Three phase flow and gravity drainage in porous media," *Transport in Porous Media* (1995) **20**, 77–103.
31. Piri, M. and Blunt, M.J.: "Three-dimensional mixed-wet random pore-scale network modeling of two- and three-phase flow in porous media. I. Model description," Submitted to Phys. Rev. E (2004).
32. van Dijke, M.I.J. and Sorbie, K.S.: "Three-phase capillary entry conditions in pores of noncircular cross-section," *J. Coll. Int. Sci.* (2003) **260**, 385–397.
33. van Dijke, M.I.J., Lago, M., Sorbie, K.S., and Arujo, M.: "Free energy balance for three fluid phases in a capillary of arbitrarily shaped cross-section: capillary entry pressures and layers of the intermediate-wetting phase," *J. Coll. Int. Sci.* (2004) **277**, 184–201.
34. Piri, M. and Blunt, M.J.: "Three-phase threshold capillary pressures in non-circular capillary tubes with different wettabilities including contact angle hysteresis," Submitted to Phys. Rev. E (2004).
35. Whitson, C.H. and Brulè, M.R.: *Phase Behavior*, Henry L. Doherty series Monograph / SPE Series, Society of Petroleum Engineers, Richardson, TX (2000) **20**.

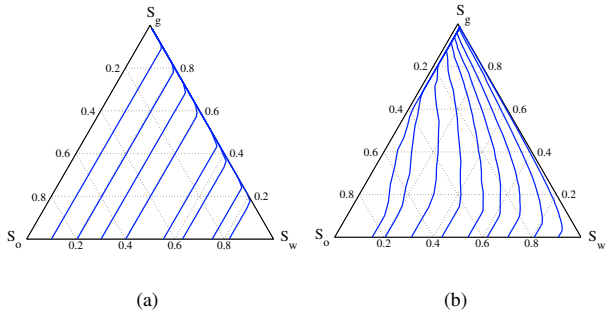

Figure 4: Saturation trajectories for (a) the water-wet case and (b) the oil-wet case.

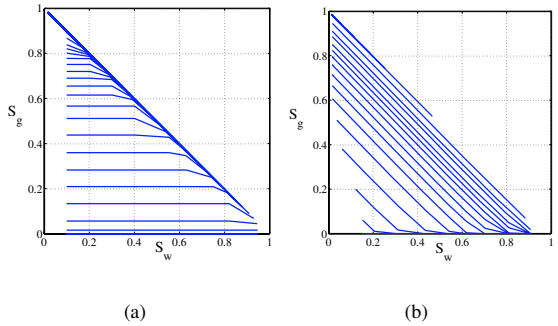

Figure 5: Gas-oil iso-capillary pressure curves for (a) the water-wet case and (b) the oil-wet case.

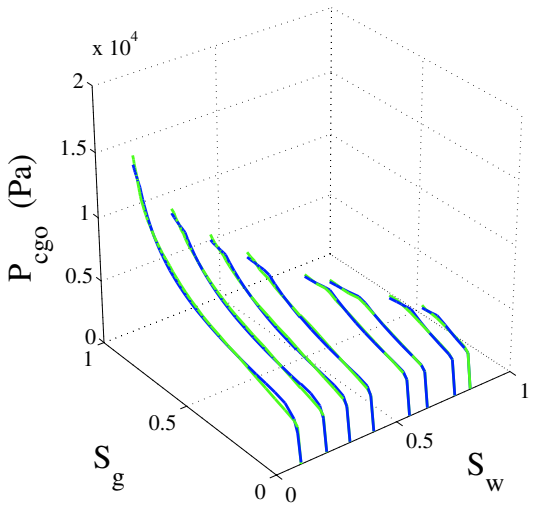

(a)

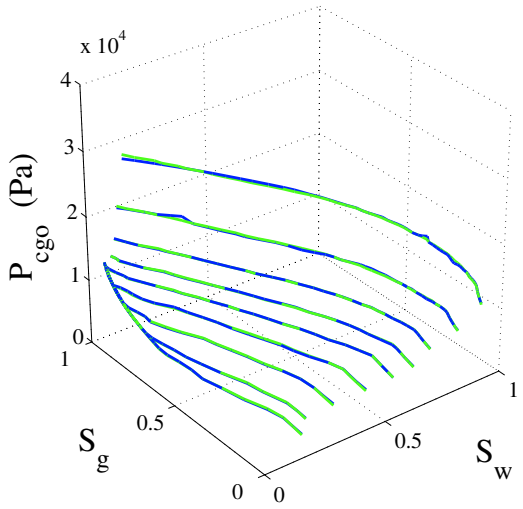

(b)

Figure 6: Gas-oil capillary pressure curves for (a) the water-wet case and (b) the oil-wet case. The computed curves are shown in green, while the correlations are shown in blue.

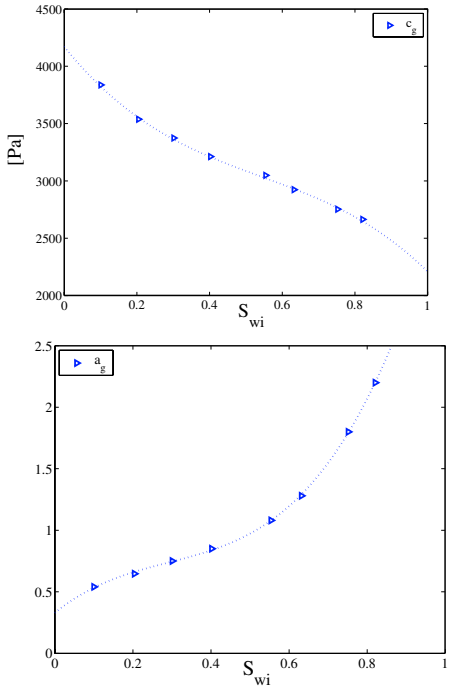

Figure 7: The correlation parameters fitted to third-order polynomials for the water-wet case.

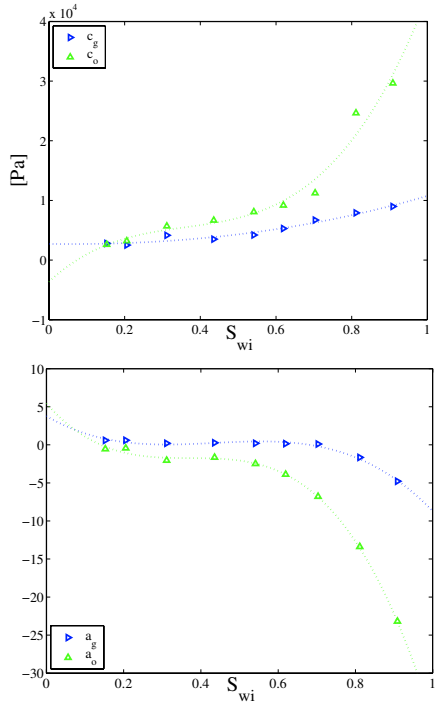

Figure 8: The correlation parameters fitted to third-order polynomials for the oil-wet case.

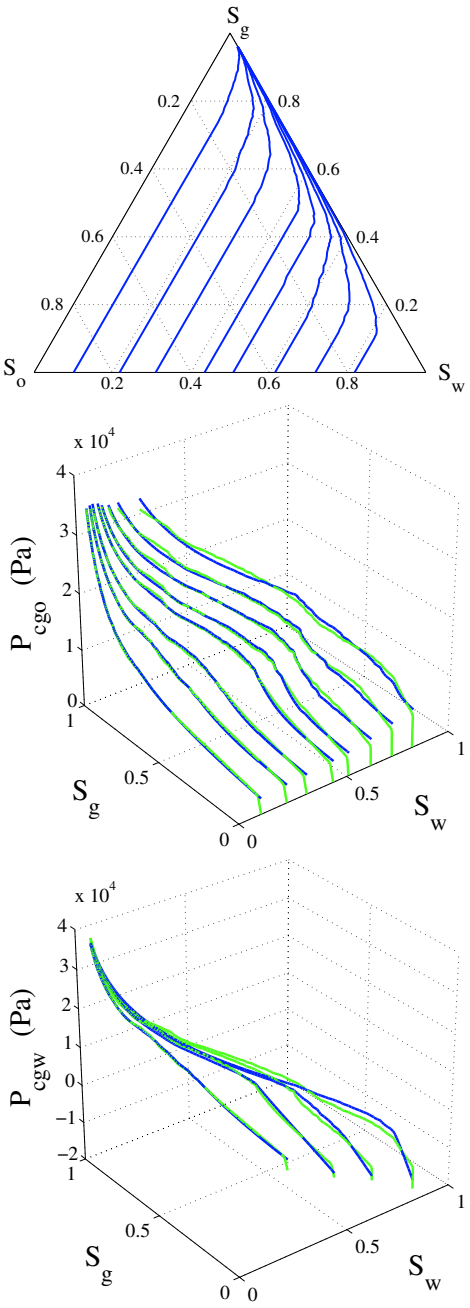

Figure 9: Displacement paths and capillary pressure curves for gas invasion, mixed-wet conditions. The computed curves are shown in green, and the correlations are shown in blue.

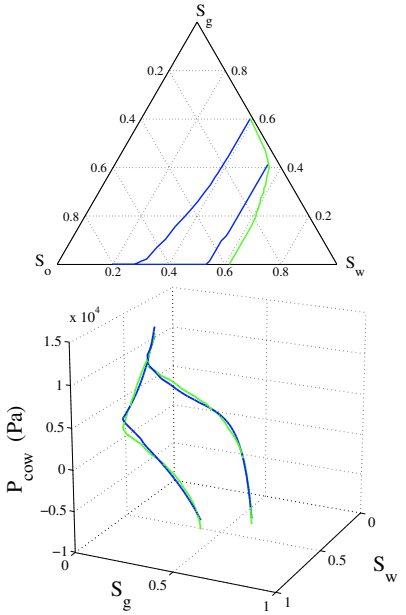

Figure 10: Displacement paths and capillary pressure curves for the DID processes, mixed-wet conditions. The computed curves are shown in green, and the correlations are shown in blue.

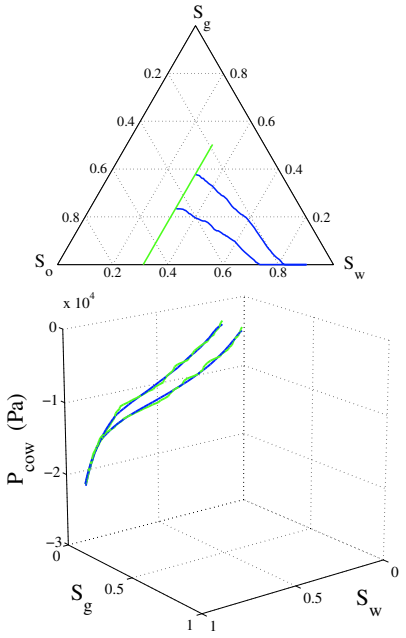

Figure 11: Displacement paths and capillary pressure curves for the IDD processes, mixed-wet conditions. The computed curves are shown in green, and the correlations are shown in blue.

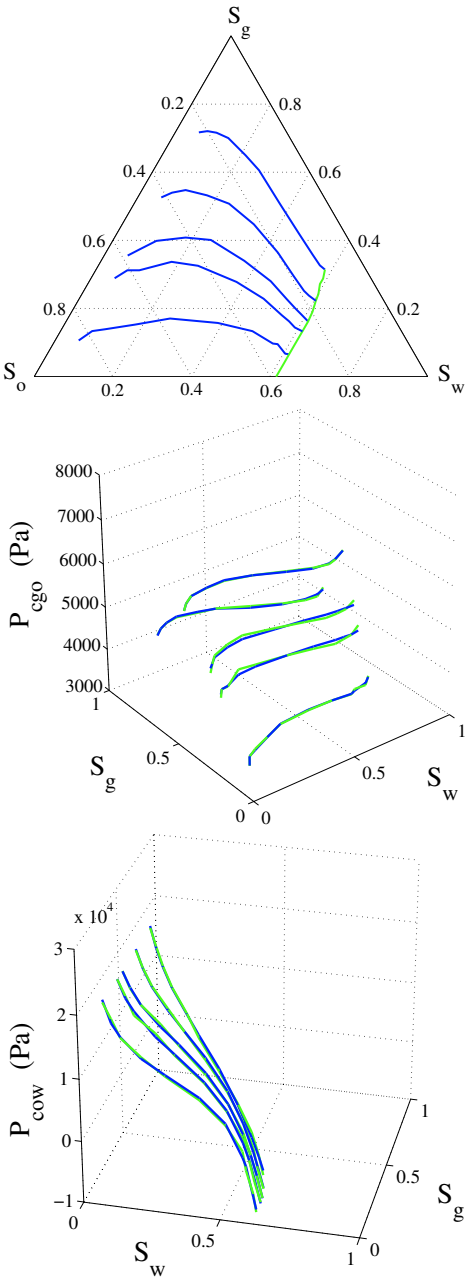

Figure 12: Displacement paths and capillary pressure curves for the DII processes, mixed-wet conditions. The computed curves are shown in green, and the correlations are shown in blue.

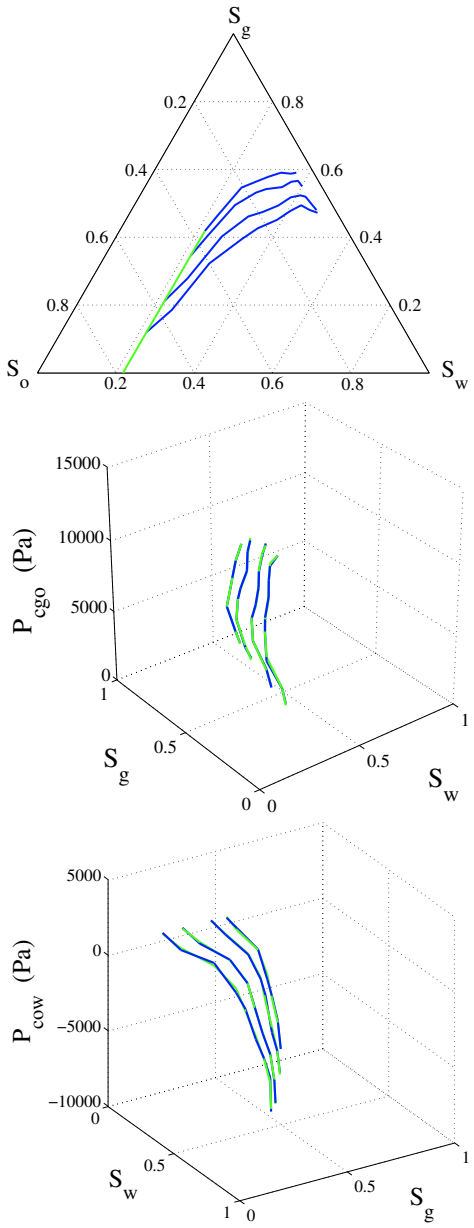

Figure 13: Displacement paths and capillary pressure curves for the IDI processes, mixed-wet conditions. The computed curves are shown in green, and the correlations are shown in blue.

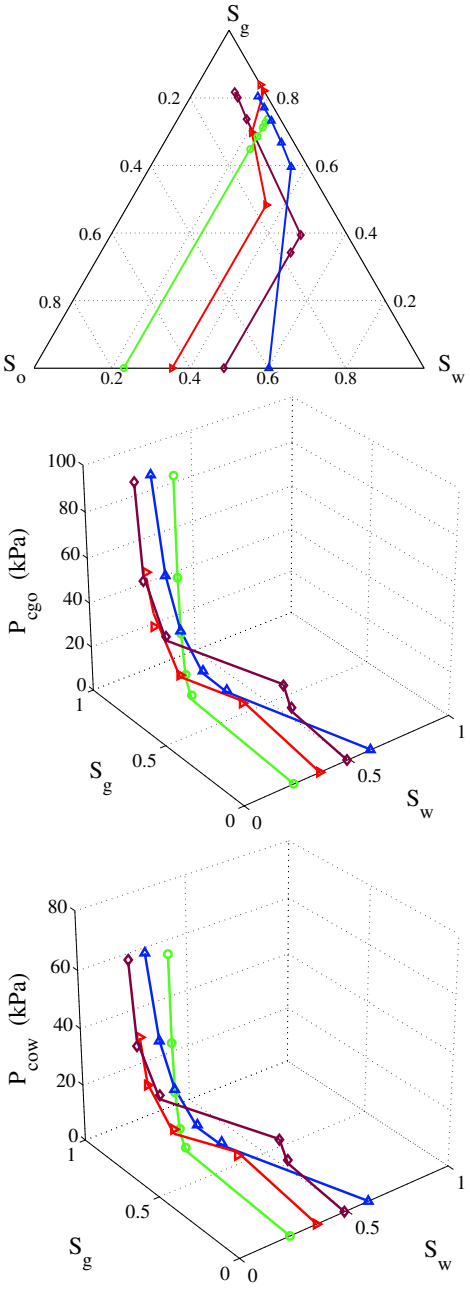

Figure 14: Displacement paths and capillary pressure curves for the drainage experiments measured by centrifuge.